Optimal Configuration of Single-Layer Domino-Coils With Uniform Spacing for Online Monitoring Equipment in Smart Grid

Yanling Li, *Member, IEEE*, Li Gui, Yongkang Jiang, Rui Jing, Yong Li, *Senior Member, IEEE*, and Zhengyou He, *Senior Member, IEEE*

***Abstract*—Domino-coils wireless power transfer (WPT) technology has emerged as an effective means of ensuring reliable power supply for online monitoring equipment in smart grid. Nonetheless, it encounters persistent challenges when integrating domino-coils into composite insulators, notably the issues of large coil size and low power transmission efficiency (PTE) over medium and long distances. In response, this article constructs a T equivalent model of domino-coils WPT system to deduce the optimal efficiency condition for any number of coils. Specifically, it is determined that PTE is maximized when the current ratio of nonadjacent coils equals the mutual inductance ratio of adjacent coils. Building upon this insight and considering practical constraints such as coil volume and transmission distance, an optimization model is formulated for single-layer domino-coils with uniform spacing under the optimal efficiency condition and given output power specification, which is subsequently determined using a particle swarm algorithm. Experimental validation is conducted utilizing a seven-coil system experiment platform, achieving an output power of 12.23 W and a PTE of 85.94% at a transmission distance of 50 cm. These findings demonstrate significant enhancements in PTE, coil volume reduction, and ease of integration into thin and uniformly distributed insulator.**

***Index Terms*—Domino-coils, online monitoring, optimal efficiency, wireless power transfer (WPT) system.**

I. Introduction

RELYING on online monitoring equipment, the smart grid ensures the efficient and safe operation of high-voltage transmission line (HVTL). With the increasing number of online monitoring equipment, attention has been drawn to the integration of wireless power transfer (WPT) technology with energy harvesters on HVTLs as a solution for stable power supply [1], [2], [3], [4], [5]. Fig. 1 illustrates an integration system for online monitoring equipment. The magnetic field energy harvester strategically positioned on the HVTL to serve as the primary power source for domino-coils WPT system. It can be maintained stably across a range of current levels by adjusting the duty cycle of MOSFETs [6], which ensures the reliable work of domino-coils WPT system. In order to facilitate installation on the power grid, the embedding of domino-coils into insulators was initially investigated in [7], as insulated repeaters for transferring power from the high voltage side to monitoring towers. In comparison to traditional power supplies utilizing storage batteries and solar cells, the input power for the domino-coils WPT system can be continuously derived from the high-voltage transmission line. Consequently, it offers advantages such as low maintenance costs and independence from weather conditions.

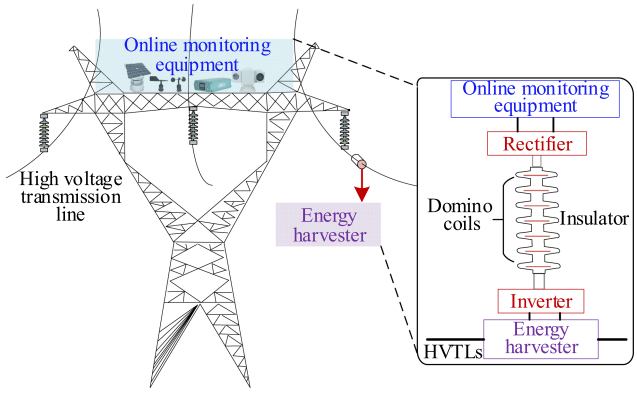

Fig. 1. WPT system with domino-coils for online monitoring equipment.

The domino-coils of WPT system are also referred to as multiple-relay coils, which are compensated by external resonant capacitors or self-resonant capacitors. Numerous studies have been conducted to explore the design and optimization of domino-coils aimed at enhancing the maximum power transmission efficiency (PTE) [8], [9], [10], [13], [14], [15], [16], [17], [18], [19], [20], [21], [22], [23], [24], [25], [26], [27], [28]. According to the research by Zhang et al. [11] and Deng et al. [12], the PTE of a coil–coil WPT system is contingent upon both the coupling coefficient and the quality factor of the coils. A reduction in the coupling coefficient to less than 0.1 results in a substantial flow of current through the coil, thereby significantly impacting the PTE [18]. Furthermore, the

Manuscript received 25 March 2024; revised 15 June 2024; accepted 5 July 2024. Date of publication 11 July 2024; date of current version 11 September 2024. This work was supported in part by Sichuan Science and Technology Program under Grant 2024NSFSC0524, in part by Hebei Natural Science Foundation under Grant E2024105010, in part by the Fundamental Research Funds for the Central Universities under Grant 2682024ZTPY019, and in part by Chengdu Guojia Electrical Engineering Company, Ltd., under Grant NEEC-2022-B06. Recommended for publication by Associate Editor Rajib Centre Goswami. *(Corresponding author: Yanling Li.)*

The authors are with the School of Electrical Engineering, Southwest Jiaotong University, Chengdu 611756, China (e-mail: yanling_li@swjtu.edu.cn; swjtu_gl@my.swjtu.edu.cn; jiangyongkang@my.swjtu.edu.cn; jingrui@my.swjtu.edu.cn; yong_li@swjtu.edu.cn; hezy@home.swjtu.edu.cn).

Color versions of one or more figures in this article are available at https://doi.org/10.1109/TPEL.2024.3426589.

Digital Object Identifier 10.1109/TPEL.2024.3426589

skin effect and proximity effect experienced by coil windings at high frequencies elevate the equivalent series resistance of the coil, leading to a reduction in the quality factor that also exerts a significant influence on the PTE through ohmic dissipation.

In HVTL applications, the weight and volume of domino-coils need to satisfy the strict restrictions. In comparison to cylindrical solenoid couplers as discussed in [19] and [20], planar domino-coils with high power density offer enhanced suitability for transmission line applications. Consequently, extensive research has been conducted on the structure and dimensions of planar domino-coils to improve the coupling coefficient and quality factor of the coils. Among the various structures studied, multilayer coils have received considerable attention. Qu et al. [21] proposed the utilization of two-layer PCB coils compensated by parasitic capacitance to confine the size of resonators. By adjusting the trace width of PCB coils, the quality factor could be increased from 45 to 64, achieving a maximum PTE of 11% over a transmission distance of 1.14 m. Fang et al. [22] developed a simulation-driven optimization framework employing Bayesian algorithms to enhance the quality factor of PCB resonators. Through adjustments in track width, spacing, and maximal self-resonant frequency, they achieved a quality factor of up to 132, with a corresponding improvement in PTE to 46% in a 20 W prototype. Zhou et al. [23] designed a hybrid structure with single-layer PCB (applied for the transmitter and receiver coils) and two-layer PCB (applied for the three relay resonators in the middle). This design achieved a resonant frequency exceeding 1 MHz, a quality factor of about 144, and a maximum PTE of 55.2% over a transmission distance of 380 mm. However, it is worth noting that due to the serious skin effect and proximity effect of solid conductors in high frequencies, achieving significant improvements in the quality factor of PCB coils proves challenging, and the ohm dissipation continues to dominate total power losses.

Previous studies have determined that Litz wire coils with stranded conductors exhibit a higher quality factor when contrasted with PCB coils. Based on the 3.4 mm total thickness of two-layer Litz wire coils, the quality factor was about 300, and more than 60% PTE was achieved at a transmission distance of 1.1 m [1]. Furthermore, by using the thicker coils with three-layer and 14 mm total thickness, both the coupling coefficient and the quality factor increased with the maximum value of 0.14, 350, respectively [13]. Although the coupling coefficient and the quality factor can be reasonably high by increasing the coil thickness and/or diameter, practical application scenarios often impose constraints against such adjustments. Thus, apart from coil dimension, the influence of the number and distance of relay coils on system's coupling coefficient and overall PTE was investigated in [18]. Lee and Chae [24] observed that the quality factor of coil resonators has a strong influence on determining their optimal positions. They derived the optimal coupling coefficient between Tx and the first relay coil for given placements of the remaining coils. However, only three coil resonators were considered in their analytical model with the cross coupling neglected. The effects of the cross coupling of nonadjacent coils for five and six domino-coils were explored in [25], revealing that it could enhance the PTE by slightly shifting away from the resonance frequency. Meanwhile unequal-spaced domino-coils demonstrated higher overall PTE compared to equal-spaced configurations. Additionally, a transfer coefficient model of five domino-coils was proposed in [26] and [27] to further analyze the effect of cross-coupling on coil current and power transfer paths. Guan et al. [28] studied the optimal spaced coil strategy to improve PTE by adjusting the distance between adjacent coils, and a significant improvement of 27.2% at a load of 100 Ω was achieved.

Even though previous works studied various novel analysis for designing domino-coils, most of them improved the PTE by using multilayer Litz coils or optimizing the spacing distance between adjacent coils. However, embedding the proposed domino-coils into composite insulators may not be feasible due to the following reasons: 1) the actual insulator string is uniformly distributed in space to ensure the reliable high voltage insulation, making it impractical to install these unequal-spaced coils; and 2) the thicker multilayer coils may require larger space in insulator sheets, yet the thickness of insulator sheets is limited. In this article, n-1 cascaded T-networks model of the domino-coils WPT system is constructed with the gyrator characteristics and the optimal relationship between coil current and mutual-inductance for arbitrary numbers of coils is obtained. Mathematical analysis as well as experimental verification on the optimal configuration of single-layer domino-coils are provided to demonstrate the PTE improvement.

The contributions of our work can be summarized as follows.

1) Based on the ideal maximum PTE condition where the cross-coupling is perfectly suppressed, we derive the optimal relationship between coil current and mutual-inductance, which can be universally applicable to any odd or even number domino-coils. This proposed relationship offers valuable insight into domino-coils optimization.
2) This work represents the first attempt at optimizing the configuration of single-layer domino-coils by independently adjusting each coil under the constraints of equal-spacing arrangement and maximum outer coil diameter. Optimization of individual coils is finally realized through a particle swarm algorithm.
3) The crucial coupling relation between domino-coils that determined the system PTE is analyzed. Experimental verification demonstrates the effect of cross-coupling suppression by comparing the optimal mutual-inductance ratio with the actual current ratio. This work not only optimizes the coupling coefficient and quality factor of domino-coils, but also minimizes the total space occupied by the domino-coils, effectively addressing the installation challenges of embedding coils into insulators.

The rest of this article is organized as follows. In Section II, a T-equivalent model of the domino-coils WPT system is first constructed, and then the optimal relationship between coil current and mutual-inductance is derived for arbitrary numbers of coils. Section III proposes the optimization design for single-layer domino-coils at a transmission distance of 50 cm and equal spacing based on the theoretical analysis of Section II. In Section IV, the prototype of single-layer domino-coils with

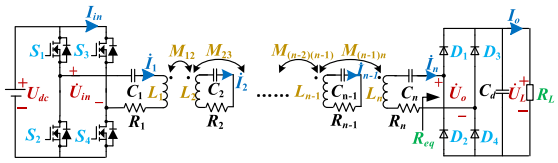

Fig. 2. Schematic of domino-coils WPT system.

equal spacing is realized, and the experiments are conducted. Finally, Section V concludes this article.

II. Modeling and Analysis

A. System Structure and Equivalent Circuit

A typical WPT system of S-topology with n domino-coils has been researched in [13]. As illustrated in Fig. 2, the dc voltage source is denoted as $U_{\rm dc}$, the load as R_L, the voltage across R_L as U_L. L_i, C_i, R_i, and I_i ($i = 12, \ldots, n$) are, respectively, the inductance, the resonant capacitance, the ac resistance, and the loop current of $i_{\rm th}$ coil. Furthermore, M_{ij} refers to the mutual inductance between $i_{\rm th}$ and $j_{\rm th}$ coil (where $j = 12, \ldots, n$; $i \neq j$). To reduce the ac resistance R_i, Litz wire is employed to wind all the domino-coils.

For modeling domino-coils WPT system, the output of inverter is equivalent to the ac source $U_{\rm in}$, and the input of rectifier is equivalent to the ac resistance R_{eq}. It has the following relationship with the load R_L [14]:

$$R_{eq} = \frac{8}{\pi^2} R_L. \tag{1}$$

According to Kirchhoff's voltage and current law, a mathematic model of WPT system can be expressed as follows:

$$\begin{bmatrix} \dot{U}_{\rm in} \\ 0 \\ 0 \\ \vdots \\ 0 \end{bmatrix} = \begin{bmatrix} Z_{11} & Z_{12} & Z_{13} & \cdots & Z_{1n} \\ Z_{12} & Z_{22} & Z_{23} & \cdots & Z_{2n} \\ \vdots & \vdots & \ddots & \vdots & \vdots \\ Z_{(n-1)1} & Z_{(n-1)2} & \cdots & Z_{(n-1)(n-1)} & Z_{(n-1)n} \\ Z_{n1} & Z_{n2} & \cdots & Z_{n(n-1)} & Z_{nn} + R_{eq} \end{bmatrix} \begin{bmatrix} \dot{I}_1 \\ \dot{I}_2 \\ \dot{I}_3 \\ \vdots \\ \dot{I}_n \end{bmatrix}. \tag{2}$$

In (2), Z_{ii} and Z_{ij} denote the self- and mutual-impedance of coils, respectively, which are defined as

$$\begin{aligned} Z_{ii} &= R_i + j(\omega_i L_i - 1/\omega_i C_i) \\ Z_{ij} &= -j\omega_i M_{ij}. \end{aligned} \tag{3}$$

Here, ω_i denotes the angular frequency of the resonant loop of each coil, which is typically designed to be identical. When the WPT system operates at resonance, the relationship between ω and circuit parameters can be expressed by

$$\omega = \omega_1 = \omega_2 = \ldots = \omega_n = \frac{1}{\sqrt{L_i C_i}}. \tag{4}$$

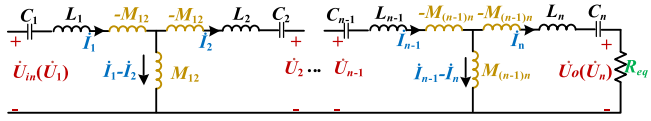

Fig. 3. Simplified circuit for the analysis of ideal maximum PTE.

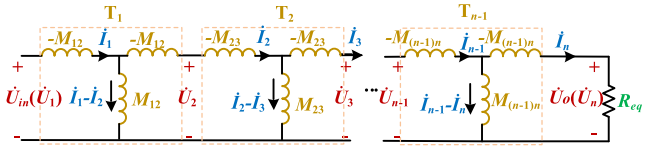

Fig. 4. T-networks with the number of n-1.

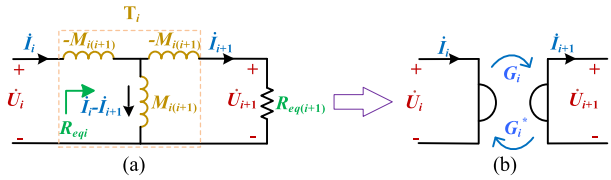

Fig. 5. Gyrator formed by T-network. (a) One T_i-network. (b) Gyrator [16].

For domino-coils, the interaction among nonadjacent coils manifests as cross-coupling, wherein reactive power exchange occurs between them, thereby influencing the system's PTE. This article adopts an innovative methodology initially considering the scenario from a reverse standpoint, wherein cross-coupling is assumed to be entirely mitigated, and the ac resistance of domino-coils is sufficiently negligible to be as zero. Subsequently, the relationship between circuit parameters is deduced in reverse, which is regarded as the ideal maximum PTE condition.

Drawing upon the aforementioned assumption, a simplified circuit is derived, as illustrated in Fig. 3. When the parameters L_i and C_i of each coil loop adhere to condition (4), the circuit can be further simplified as Fig. 4 , by utilizing the T-type equivalent circuit method, as described in [15]. And then, the domino resonators are finally equivalent to n-1 cascaded T-networks.

Consequently, the equivalent circuit of the WPT system can be finally expressed by

$$\begin{bmatrix} \dot{U}_{\rm in} \\ 0 \\ 0 \\ \vdots \\ 0 \end{bmatrix} = \begin{bmatrix} 0 & Z_{12} & 0 & \cdots & 0 \\ Z_{12} & 0 & Z_{23} & \cdots & 0 \\ \vdots & \vdots & \ddots & \vdots & \vdots \\ 0 & 0 & Z_{(n-2)(n-1)} & 0 & Z_{(n-1)n} \\ 0 & 0 & 0 & Z_{(n-1)n} & R_{eq} \end{bmatrix} \begin{bmatrix} \dot{I}_1 \\ \dot{I}_2 \\ \dot{I}_3 \\ \vdots \\ \dot{I}_n \end{bmatrix}. \tag{5}$$

In accordance with the reverse derivation concept, as (5) delineates the parameter constraint relationship under optimal efficiency transmission. The general solution of (5) is influenced by the total number of domino-coils, resulting in disparate expressions for coil currents when n is even as opposed to when n is odd.

B. Optimal Efficiency Condition

In order to more effectively find the relationship between the coil currents and circuit parameters, it is valuable to research the characteristics of T-networks with the number of n-1 in Fig. 4.

The present work introduces a graphical design method predicated upon the distinctive attributes of the gyrator [16]. A gyrator, characterized as a two-port element, is elucidated for its capability to convert voltage from one port into current at another, or vice versa.

The characteristic feature of a gyrator enables the conversion between voltage and current sources, as expressed by equation [17]

$$\begin{bmatrix} \dot{I}_i \\ \dot{I}_{i+1} \end{bmatrix} = \begin{bmatrix} 0 & {G_i}^* \\ G_i & 0 \end{bmatrix} \begin{bmatrix} \dot{U}_i \\ \dot{U}_{i+1} \end{bmatrix} \tag{6}$$

where G_i and ${G_i}^*$ represent conjugate complex numbers, denoting the forward and reverse trans-conductance of the gyrator, respectively.

In the context of a resonant T-network within domino-resonators satisfying the impedance condition of the gyrator, the analysis of domino-resonators in WPT system can be conducted based on the conversion properties of the gyrator shown in Fig. 5.

The forward and reverse trans-conductance of an independent T_i-network is represented by

$$\begin{cases} G_i = \frac{1}{j\omega M_{i(i+1)}} \\ G_i^* = -\frac{1}{j\omega M_{i(i+1)}}. \end{cases} \tag{7}$$

Utilizing (6), the expressions for the input and output impedance of the T_i-network are derived, as presented in

$$\begin{cases} R_{eqi} = \frac{U_i}{I_i} = \frac{I_{i+1}/G_i}{U_{i+1}G_i^*} \\ R_{eq(i+1)} = \frac{U_{i+1}}{I_{i+1}} = \frac{I_i/{G_i}^*}{I_{i+1}}. \end{cases} \tag{8}$$

Here, the input impedance R_{eqi} of the T_i-network corresponds to the output impedance of $T_{i\text{-}1}$-network, and the output impedance $R_{eq(i+1)}$ of the T_i-network corresponds to the input impedance of T_{i+1}-network, satisfying the relationship expressed in

$$R_{eqi} = \frac{\omega^2 M_{i(i+1)}^2}{R_{eq(i+1)}}. \tag{9}$$

Building upon (7) to (9), the input and output currents of T_i-network can be expressed as

$$\begin{cases} \dot{I}_i = {G_i}^2 R_{eq(i+1)} \dot{U}_i = \frac{R_{eq(i+1)}\dot{U}_i}{\omega^2 M_{i(i+1)}^2} \\ \dot{I}_{i+1} = \frac{\dot{I}_i}{{G_i}^* R_{eq(i+1)}} = \frac{-j\omega M_{i(i+1)}\dot{I}_i}{R_{eq(i+1)}}. \end{cases} \tag{10}$$

Consequently, for the interconnected n-1 T-networks, the deduction of all currents is outlined sequentially in

$$\begin{cases} \dot{I}_1 = \frac{R_{eq2}\dot{U}_1}{\omega^2 M_{12}^2} \\ \dot{I}_2 = \frac{-j\omega M_{12}\dot{I}_1}{R_{eq2}} = \frac{-j\dot{U}_1}{\omega M_{12}} \\ \dot{I}_3 = \frac{-j\omega M_{23}\dot{I}_2}{R_{eq3}} \\ \vdots \\ \dot{I}_n = \frac{-j\omega M_{(n-1)n}\dot{I}_{n-1}}{R_{eqn}} \end{cases} \tag{11}$$

where the equivalent impedance of each coil loop satisfies

$$\begin{cases} R_{eqn} = R_{eq} \\ R_{eq(n-1)} = \frac{\omega^2 M_{(n-1)n}^2}{R_{eqn}} \\ \vdots \\ R_{eq2} = \frac{\omega^2 M_{23}^2}{R_{eq3}}. \end{cases} \tag{12}$$

From the general current expression in (11), it is observed that the current phase difference successively lags by 90° for the domino-coils with total number of n. The currents flowing through the odd-numbered coils are contingent upon n, which may be either odd or even, owing to the distinct relationship between R_{eq2} and R_{eqn} that is related to n.

Then, the output power of domino-coils WPT system can be obtained in (13) according to the current expression. When the coils number n is even or odd, the output power is denoted as $P_{o\text{·even}}$ and $P_{o\text{·odd}}$, respectively, as follows:

$$\begin{cases} P_{o\_\text{even}} = I_n^2 R_{eq} = \frac{R_{eq}U_{\text{in}}^2}{\omega^2} \frac{\prod_{k=n/2-1,\cdots,2,1} M_{(2k)(2k+1)}^2}{\prod_{k=n/2,n/2-1,\cdots,2,1} M_{(2k-1)(2k)}^2} \\ P_{o\_\text{odd}} = I_n^2 R_{eq} = \frac{U_{\text{in}}^2}{R_{eq}} \frac{\prod_{k=(n-1)/2,\cdots,2,1} M_{(2k)(2k+1)}^2}{\prod_{k=(n-1)/2,\cdots,2,1} M_{(2k-1)(2k)}^2}. \end{cases} \tag{13}$$

And for the adjacent T-network T_{i+1} (i = 1,…,n-2) in domino-resonators, the voltage and current also has the similar relationship

$$\begin{bmatrix} \dot{I}_{i+1} \\ \dot{I}_{i+2} \end{bmatrix} = \begin{bmatrix} 0 & {G_{i+1}}^* \\ G_{i+1} & 0 \end{bmatrix} \begin{bmatrix} \dot{U}_{i+1} \\ \dot{U}_{i+2} \end{bmatrix}. \tag{14}$$

Despite the disparity in output features between odd and even domino-coil numbers, the two adjacent T-networks consistently operate under the condition specified in (15) by combining (6) and (14)

$$\begin{cases} \frac{I_i}{I_{i+2}} = \left|\frac{{G_i}^*}{G_{i+1}}\right| = \frac{M_{(i+1)(i+2)}}{M_{i(i+1)}} = S_i \\ \frac{U_i}{U_{i+2}} = \left|\frac{{G_{i+1}}^*}{G_i}\right| = \frac{M_{i(i+1)}}{M_{(i+1)(i+2)}} = 1/S_i \end{cases}, i = 1, \cdots, n-2. \tag{15}$$

Here, S_i is defined as the mutual inductance ratio of adjacent coils. Notably, in two adjacent T-networks, the current ratio of I_i to I_{i+2} equals to the mutual inductance ratio of $M_{(i+1)(i+2)}$ to $M_{i(i+1)}$, or the voltage ratio of U_i to U_{i+2} is inversely proportional to the mutual inductance ratio of $M_{(i+1)(i+2)}$ to $M_{i(i+1)}$. As long as the above relationship is satisfied, the domino-coils WPT system will realize the ideal maximum PTE.

III. Optimization Method

A. Optimization Model and Design Flow

To make the domino-coils WPT system operates at the state of ideal maximum PTE, adjustments can be made to the domino-coils structure to satisfy the relationship outlined in (15). In comparison to configurations involving unequal spacing and multilayer domino-coils, the optimization favors single-layer domino-coils with uniform spacing. Initially, two indices, denoted as f_1 and f_2, are defined, where f_1 represents the average disparity between the current ratio and the mutual inductance ratio, while f_2 signifies the discrepancy between the output power P_o and a reference value P_{ref}. To achieve the maximum PTE given the desired output power, the optimization objective aims to minimize the combined value of f_1 and f_2, expressed as

$$f = \min(f_1 + f_2), \begin{cases} f_1 = \frac{1}{n-2} \sum_{i=1}^{n-2} \left| \frac{I_i}{I_{i+2}} - \frac{M_{(i+1)(i+2)}}{M_{i(i+1)}} \right| \\ f_2 = (P_o - P_{ref})/P_{ref} \end{cases}. \tag{16}$$

For the power supply of the online monitoring equipment, domino-coils are typically positioned within the insulation shed with uniform spacing to ensure optimal insulation properties. However, due to spatial constraints, the size of the coils must not exceed the external diameter of the insulation shed. Consequently, the optimization objective under equal spacing for single-layer domino-coils is subject to certain constraint conditions, as illustrated in

$$\begin{cases} 5 \le n \le 10 \\ h = d_{\text{given}}/(n-1) \\ 2\text{mm} \le w_g \le 5\text{mm} \\ 1 \le N_i \le (r_{out} - r_{in})/w_g + 1, i = 1, 2, \ldots, n, N_i \in N^+ \\ 1\Omega \le R_{eq} \le 500\Omega \\ 5\text{V} \le U_{\text{in}} \le 50\text{V}. \end{cases} \tag{17}$$

Here, the number of single-layer domino-coils, denoted as n, is directly linked to the quantity of insulation sheds, and the values of n in the range of 5 to 10 is investigated in this work. The parameter d_{given} represents the transmission distance and is interconnected with the insulation distance, and the air gap h between the coils can be computed based on d_{given} and n. The spacing w_g between coil turns, particularly when wound tightly with Litz wire, aligns with the Litz wire diameter w_d. However, considering the coupling coefficient when the Litz wire is loosely wound, w_g should not surpass certain upper limit of 5 mm. Furthermore, r_{in} and r_{out} are the inner and outer radii of the coil, determined by the outer diameter of the core rod and the insulation shed, respectively. N_i is the turn number of the i_{th} coil, and its maximum value must adhere to the constraint imposed by w_g, r_{in}, and r_{out}. Additionally, the equivalent load R_{eq} and input voltage U_{in} are used as the optimization parameters to achieve the power matching, with their ranges set as [1 Ω, 500 Ω] and [5 V, 50 V], respectively. With the common-used frequency of hundreds of kHz in domino-coils WPT system, a specific frequency of 500 kHz is employed in this study. Due to the online monitoring equipment as a power supply object of WPT system, its average power dissipation ranges between 10 W and 20 W, and a reference value P_{ref} is set at 12 W. The range of variable parameters and the values of fixed parameters are detailed in Table I.

TABLE I
Parameter Setting

Symbol	Meaning	Variable or fixed	Range
n	Number of coils	Variable	[5,10]
w_g	Turn spacing	Variable	[2,5]mm
N_i	Number of coil turns	Variable	[1, (r_{out} - r_{in})/ w_g +1]
R_{eq}	Equivalent load	Variable	[1500]Ω
U_{in}	Input voltage	Variable	[550]V
w_d	Litz wire diameter	Fixed	2 mm
h	Air gap of coils	Fixed	8.33 cm
r_{in}	Inner radius of coils	Fixed	1 cm
r_{out}	Outer radius of coils	Fixed	10 cm
d_{given}	Transmission distance	Fixed	50 cm
f	Operating frequency	Fixed	500 kHz
P_{ref}	Reference output power	Fixed	12 W

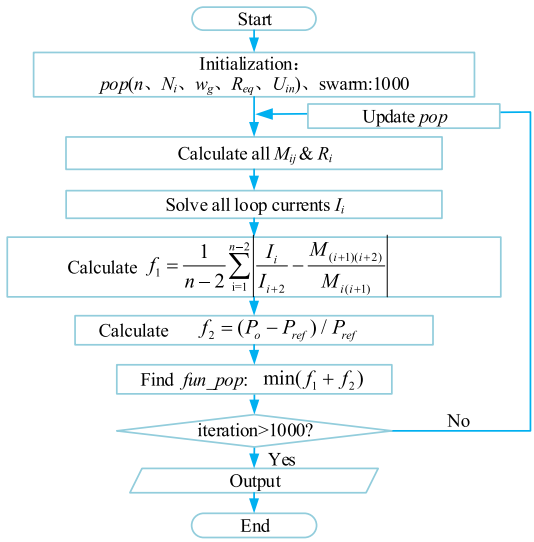

Fig. 6. Flow chart of PSO algorithm.

The variables, namely n, N_i, w_g, R_{eq}, and U_{in}, are optimized using the particle swarm optimization (PSO) algorithm to attain optimal efficiency under the specified output power P_{ref}. MATLAB is employed for the computation of mutual inductance and ac resistance of single-layer domino-coils across various values of n, N_i, w_g, R_{eq}, and U_{in}, facilitating the PSO optimization process. The flow chart outlining this process is depicted in Fig. 6.

First, both the initial population size and the number of iterations are set to 1000. The variables n, N_i, w_g, R_{eq}, and U_{in} are initialized to ensure comprehensive coverage of the initial population within the specified value ranges. Subsequently, based on the calculation method in [30] and [25], the mutual inductance M_{ij} and ac resistance R_i are calculated, followed by the solution of the current of each loop using (11). Thereafter, f_1, f_2, and f in (16) are computed. The minimum f among the 1000 results is identified and designated as *fun_pop*, with the corresponding parameter combination denoted as *pop*, including n, N_i, w_g, R_{eq}, and U_{in}. By exploring values around the parameter combination *pop*, further refinement of the value range is conducted, initiating

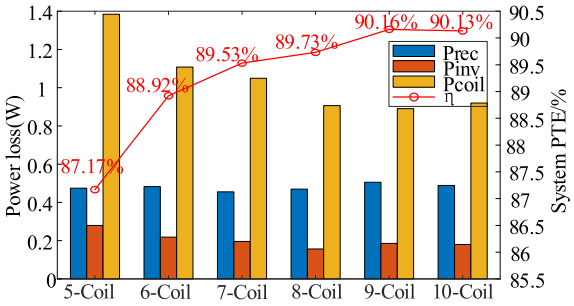

Fig. 7. Efficiency and power loss of domino-coils WPT system.

the first iteration. A new minimum f is then selected, and a new dataset *pop* is obtained. This iterative process continues until the specified maximum number of iterations is reached. Ultimately, after 1000 iterations, the fitness function f approaches the global optimum, yielding the coil parameter combination that meets the predetermined requirements. The computer configuration utilized in this study is equipped with an AMD Ryzen 7 5800H processor and 16 GB of Random Access Memory. Utilizing MATLAB for programming and computational tasks, the entire process is estimated to require approximately one hour to complete.

B. Optimization Analysis

Based on the optimization process, the study observes the system PTE and power loss across a range of 5 to 10 domino-coils, as illustrated in Fig. 7. Power dissipation arises from multiple sources including the inverter, rectifier, and the coils themselves, all of which have the potential to diminish the PTE. Notably, the analysis highlights that the predominant factor contributing to power loss is coil resistance. For instance, in a system utilizing five domino-coils, the PTE registers at 87.17%. Subsequently, with an increase to seven domino-coils, a discernible enhancement in PTE is observed, reaching 89.53%. However, beyond seven domino-coils, the incremental improvement in PTE becomes less pronounced.

In Fig. 8, we illustrate the iterative process of coil turns N_1–N_7 and the equivalent load R_{eq} under the condition of $n = 7$. The horizontal axis represents the number of iterations, while the vertical axis denotes N_1–N_7 and R_{eq}, respectively. As the setting in (17), N_1–N_7 are constrained to positive integers, thus, they are iterated accordingly. R_{eq} is allowed to vary arbitrarily within the specified range. Notably, the data points cluster along a nearly linear trajectory, indicating the optimal values in the iterations. Table II provides a summary of optimal values derived from this process. Additionally, S_1–S_5 are further calculated based on the optimal values of coil parameters.

To assess the impact of S_1–S_5 on the system PTE, the initial turns of the domino-coils are all set to be equal. Subsequently, N_1 is gradually reduced while N_3 is correspondingly increased, resulting in an increase in S_1 (M_{23}/M_{12}). This process allows us to observe the variation in system PTE with respect to S_1–S_5, as depicted in Fig. 9. Notably, the optimized values of S_1–S_5 from Table II are highlighted on the curve. It is evident that S_1, S_2, S_3,

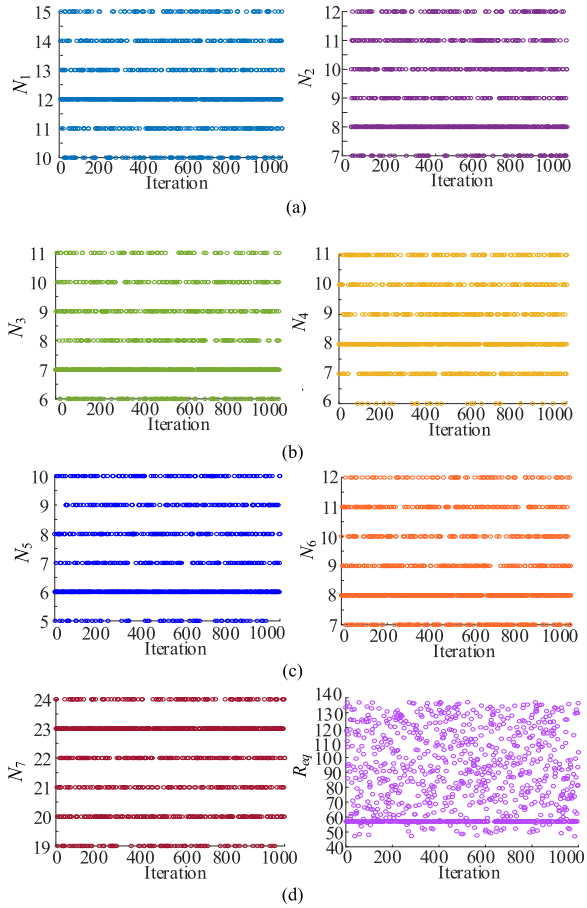

Fig. 8. Iteration process for (a) N_1 and N_2, (b) N_3 and N_4, (c) N_5 and N_6, and (d) N_7 and R_{eq}.

TABLE II
OPTIMAL VALUE OF VARIABLE PARAMETERS

Symbol	Optimal value
w_g	3 mm
N_1	12
N_2	8
N_3	7
N_4	8
N_5	6
N_6	8
N_7	23
R_{eq}	57 Ω
U_{in}	16.2 V
$S_1(M_{23}/M_{12})$	0.6474
$S_2(M_{34}/M_{23})$	1
$S_3(M_{45}/M_{34})$	0.8728
$S_4(M_{56}/M_{45})$	1
$S_5(M_{67}/M_{56})$	2.5011

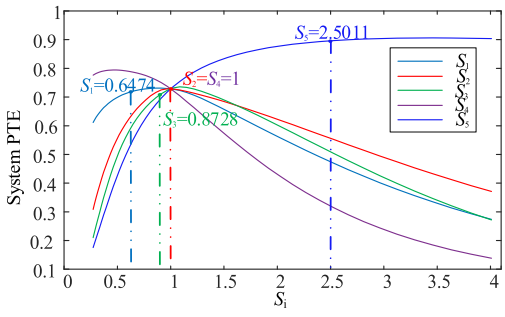

Fig. 9. System PTE versus S_i.

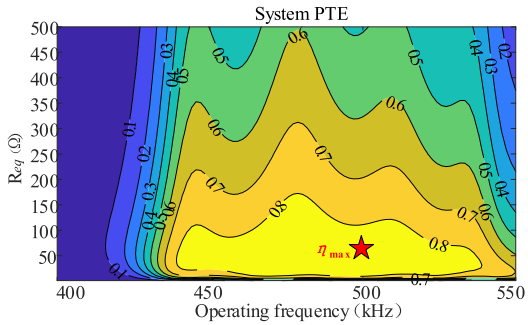

Fig. 10. PTE versus working frequency f and equivalent load R_{eq}.

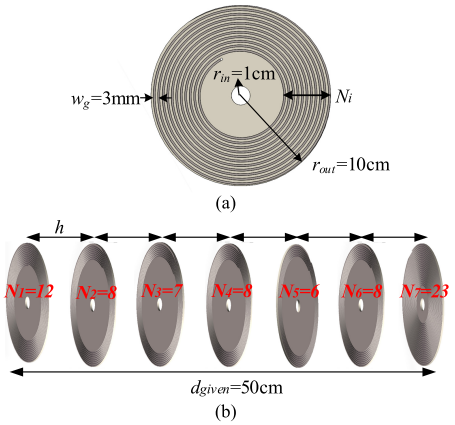

Fig. 11. Seven domino-coils proposed in article. (a) One-layer planar winding with Litz wire. (b) Uniform Spacing of domino-coils.

and S_5 closely align with the peaks of their respective efficiency curves, while S_4 has an error about 0.5.

Furthermore, in proximity to the optimal value range of S_1–S_5, the gradients of S_3 and S_4 surpass those of the respective efficiency curves for S_1, S_2, and S_5. This observation reveals the heightened sensitivity of system transmission efficiency to variations in the values of S_3 and S_4.

To further illustrate the effectiveness of the optimal load and frequency selection, the relationship between system efficiency η, operating frequency f and equivalent load R_{eq} is investigated in Fig. 10. Notably, the system efficiency surpasses 80% within the frequency range of 440 kHz to 540 kHz, indicating high PTE across this broadband spectrum, and the optimal values of operating frequency f and equivalent load R_{eq} are just located at this zone, namely $f = 500$ kHz and $R_{eq} = 57\ \Omega$.

This optimization study in Section III provides a simulation framework upon which experimental verification of optimal efficiency conditions can be built.

IV. Exprimental Validation

An experimental setup for a seven domino-coils WPT system has been constructed to validate the optimization findings. To mitigate the ohmic losses induced by skin effect, the coil is wound using Litz wire of Φ0.05 mm × 1000 strands. Fig. 11 illustrates the structure and arrangement of seven domino-coils, where coil 1 serves as the transmitting coil, coils 2–6 act as relay coils and coil 7 functions as the receiving coil. All coils have an outer radius of 10 cm, an inner radius of 1 cm, and a 3 mm air gap between coil turns. With a power transmission distance of 50 cm, the number of turns for coils 1–7 are 12, 8, 7, 8, 6, 8, and 23, respectively.

TABLE III
Parameters of All Coils

Symbol	Value	Unit
L_1–L_7	35.23/19.95/16.72/20.13/ 13.3/20.33/67.72	μH
R_1–R_7	0.16/0.116/0.104/0.123/0.096/ 0.123/0.28	Ω
C_1–C_7	2.935/4.635/5.405/5.2/6.9/4.935/5.4	nF
Q_1–Q_7	691/540/505/515/436/519/759	/
$K_{12}/K_{23}/K_{34}/K_{45}/K_{56}/K_{67}$	0.154/0.142/0.141/0.139/0.129/0.154	/
$M_{12}/M_{23}/M_{34}/M_{45}/M_{56}/M_{67}$	4.102/2.607/2.592/2.287/2.132/5.742	μH
$M_{13}/M_{24}/M_{35}/M_{46}/M_{57}$	1.085/0.815/0.582/0.82/1.155	μH
$M_{14}/M_{25}/M_{36}/M_4$	0.387/0.202/0.3/0.595	μH
$M_{15}/M_{26}/M_{37}$	0.145/0.165/0.23	μH
M_{16}/M_{27}	0.11/0.075	μH
M_{17}	0.075	μH

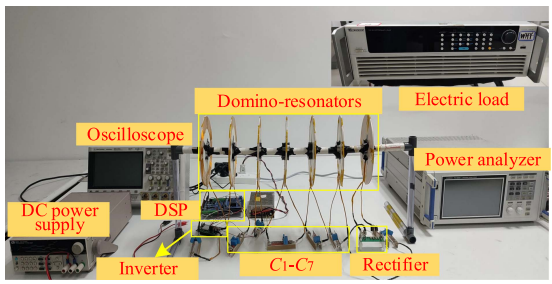

Fig. 12. Experiment platform.

Table III presents the parameters of seven domino-coils WPT system, including the self-inductance, mutual inductance, ac resistance, and resonant capacitance. Additionally, it calculates the quality factor and coupling coefficient between adjacent coils. Notably, the maximum quality factor in seven domino-coils is $Q_7 = 759$, while the maximum coupling coefficient is are K_{12} and $K_{67} = 0.154$.

The experiment platform of seven domino-coils WPT system with a total transmission distance of 50 cm is shown in Fig. 12. The experimental apparatus comprises various instruments and equipment, notably including dc power supply, DSP, inverter, rectifier, electronic load, domino-resonators, oscilloscope, and power analyzer.

The steady state of system is first tested in experiment. Fig. 13 illustrates the system input voltage and current waveforms, with a resonant frequency of 498.4 kHz. In this figure, $u_{\rm in}$ represents the output voltage of the inverter, and the dc input voltage $U_{\rm dc}$ is maintained at 20 V. The output current of the inverter, denoted as i_1, has an rms value of 1.095 A, with a phase lag of 28° relative to $u_{\rm in}$. Additionally, the waveforms of V_{ds} (drain-source voltage) and V_{gs} (gate voltage) of one MOSFET in the inverter are presented in the bottom-left corner of Fig. 13(a). It is observed that when V_{gs} rises to 5 V, V_{ds} drops to 0 V, indicating that the MOSFETs in the inverter achieve zero voltage switching. Furthermore, Fig. 13(b) and (c) display the current waveforms of coils 1–7. These waveforms reveal that the currents from

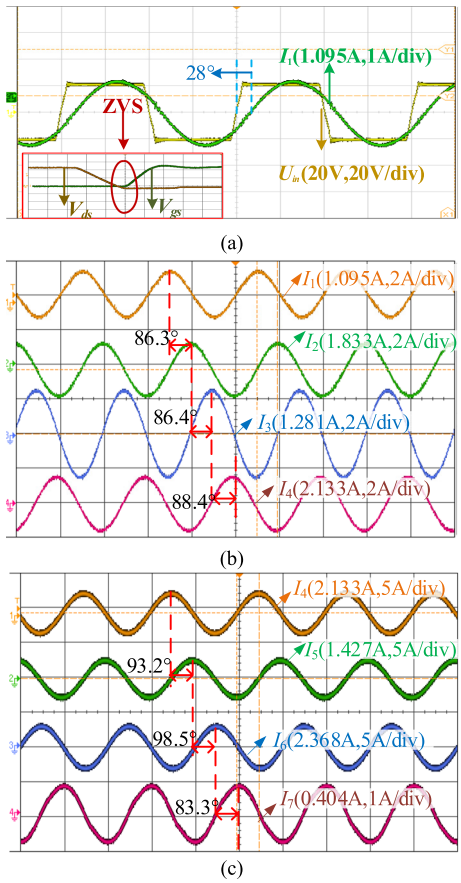

Fig. 13. Steady waveforms of the voltage and current. (a) Input voltage u_{in} and current i_1. (b) Steady currents of i_1–i_4. (c) Steady currents of i_4–i_7.

I_1 to I_7 lags in phase by 86.3°, 86.4°, 88.4°, 93.2°, 98.5°, and 83.3°, successively. Upon comparison with theoretical analysis, the actual lags in current phase exhibit a maximum deviation of 8.5° from the expected 90°. These results demonstrate that while the method proposed in this article effectively mitigates cross-coupling to some extent, it does not entirely eliminate cross-coupling among the domino-coils.

To validate the effectiveness of the single-layer domino-coils design, the system's transmission power and efficiency are measured with a fixed input voltage of $U_{\text{dc}} = 20$ V while varying the load value R_L, as illustrated in Fig. 14(a). It is evident from the graph that the system consistently achieves more than 80% PTE across the load range of 45–110 Ω. The transmission efficiency first increases and then decreases as the load value changes. The maximum system efficiency is observed at a load of $R_L = 80$ Ω, reaching 85.94%, corresponding to an output power of 12.23 W. Furthermore, experiments are conducted with a fixed load value of $R_L = 80$ Ω while varying the input voltage from 5 V to 25 V, as illustrated in Fig. 14(b). As a result, the system's output power increases from 0.72 W to 19.6 W, and the transmission efficiency rises from 79.62% to 86.33%. Compared to the optimized design index for domino-coils WPT system in (16), the reference output power has been satisfied at the input voltage of $U_{\text{dc}} = 20$ V and the load of $R_L = 80$ Ω.

Moreover, the transmission efficiency under this working point reaches the maximum value of 85.94%. A screenshot of the

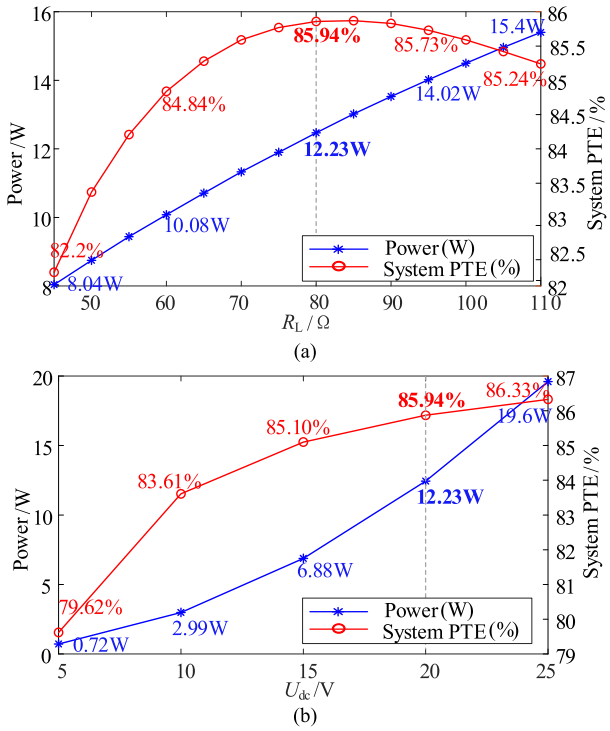

Fig. 14. System PTE and output power versus (a) different R_L and (b) different U_{dc}.

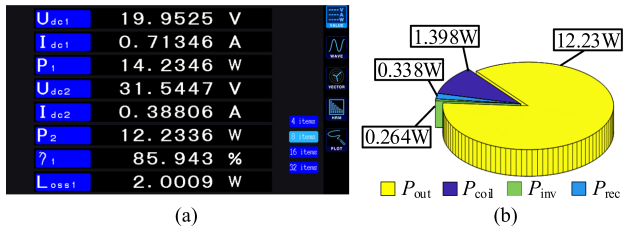

Fig. 15. Power loss analysis under maximum PTE. (a) Screenshot of power analyzer. (b) Power distribution.

power analyzer for seven domino-coils WPT system is provided in Fig. 15(a), indicating an input power of 14.23 W and an output power of 12.23 W with a total loss of 2 W. Fig. 15(b) further dissects the power losses of each component in the system. The ohmic dissipation resulting from coil resistance accounts for 1.398 W, while the inverter and rectifier losses amount to 0.264 W and 0.338 W, respectively. It can be seen that the ohm dissipation is the main source of power losses.

This work focuses on enhancing system efficiency by optimizing the parameters of single-layer domino-coils structure to suppress the cross-coupling between coils. The theoretical analysis reveals that the equivalence between the mutual inductance ratio and the current ratio determines the maximum PTE of domino-coils WPT system. Utilizing the measured data on mutual inductance between adjacent coils and the loop current of each coil, we calculate the current ratio I_i/I_{i+2} and the mutual inductance ratio $M_{(i+1)(i+2)}/M_{i(i+1)}$, where $i = 12, 34, 5$ in 7 domino-coils WPT system. The results are displayed in Fig. 16, the blue and cyan bars representing $M_{(i+1)(i+2)}/M_{i(i+1)}$ and I_i/I_{i+2}, respectively, while the red line indicates the deviation

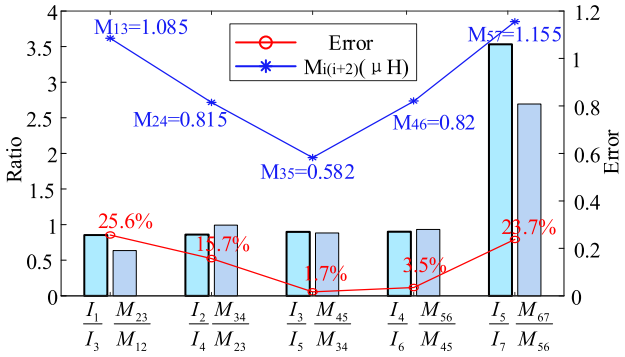

Fig. 16. Deviation of current ratio and mutual inductance ratio.

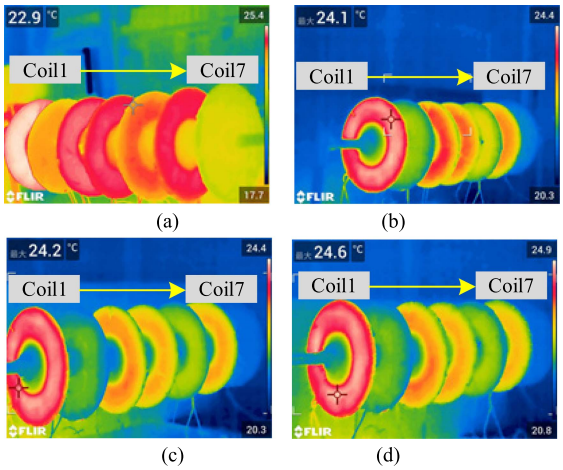

Fig. 17. Temperature rise of coil in every half-hour. (a) 20:50 P.M. (b) 21:20 P.M. (c) 21:50 P.M. (d) 22:20 P.M.

between $M_{(i+1)(i+2)}/M_{i(i+1)}$ and I_i/I_{i+2}. The error percentages are 25.6%, 15.7%, 1.7%, 3.5%, and 23.7%, primarily concentrated in S_1, S_2, and S_5. Examining the distribution of cross-coupling $M_{i(i+2)}$, it reveals a consistent trend with the error curve, indicating that the deviation between I_i/I_{i+2} and $M_{(i+1)(i+2)}/M_{i(i+1)}$ is attributable to the cross-coupling effects. Among all the current ratios and mutual inductance ratios, S_3 and S_4 exhibit smaller errors for achieving the maximum PTE, and they reflect the crucial coupling relation in seven domino-coils WPT system. As indicated in Fig. 9, the sensitivity of system transmission efficiency to the values of S_i suggests that high-sensitivity S_i necessitates smaller errors to prevent efficiency degradation, whereas lower-sensitivity S_i allows for slightly larger errors.

In addition, taking into account the potential heating effects caused by coil ohmic dissipation during system operation, the coil temperature rise within two hours of system operation is measured, as shown in Fig. 17. From coil1 to coil 7, the temperature of coils 1, 3, 4, and 6 is slightly higher than that of coils 2 and 7, and the highest temperature is located at the transmitting coil1. It is observed that from startup until the end of the two-hour period, the coil temperatures remain stable, with an overall temperature rise of approximately 1.7 °C, which is within the allowable range.

In practical application scenarios, the transmission cable is close to the domino-coils. Therefore, the effect of the power

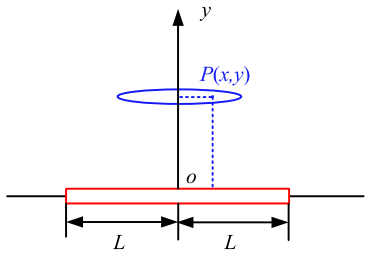

Fig. 18. Position of the coil plane relative to the cable.

frequency magnetic field (PFMF) generated by the cable on the domino-coils should be further analyzed. The PFMF induced voltage in coil is considered to be a distinct index that can reflect the influence. Because the receiving coil is far away from the cable, only the impact on transmitting coil is studied. Fig. 18 illustrates the position of transmitting coil plane relative to the cable, and y is the vertical distance for a surrounding given point $P(x, y)$ to the cable. The length of the cable is $2L$.

The length of the cable is very long relative to the size of the coil, i.e., $L \to \infty$, so it can be regarded as a long, thin, straight cable. Equation (18) gives the calculation method of magnetic flux density generated by the cable [1]

$$B_{\text{cable2coil}} = \frac{\mu_0 I_{\text{cable}}}{2\pi y} \tag{18}$$

where μ_0 is the vacuum permeability. I_{cable} is the current flowing through the cable with a magnitude of 75 A. y is equal to 0.2 m in this study. Thus, the PFMF magnetic flux flowing through the transmitting coil is

$$\begin{aligned}\phi_{\text{cable2coil}} &= N_1 \int B_{\text{cable2coil}} ds = \int_{i=1}^{N_1} \frac{\mu_0 I_{\text{cable}}}{2\pi y} d\pi r_i^2 \\ &= \frac{\mu_0 I_{\text{cable}}}{2y} \sum_{i=1}^{N_1} r_i^2 \end{aligned} \tag{19}$$

where $N_1 = 12$, and r_i is the radius of the i_{th} turn coil wound from r_{in}. It can be calculated by

$$r_i = r_{in} + (i-1)w_g + w_d/2. \tag{20}$$

The induced voltage on the transmitting coil $U_{\text{cable2coil}}$ is

$$\begin{aligned} U_{\text{cable2coil}} &= \frac{d\phi_{\text{cable2coil}}}{dt} = \frac{\mu_0}{2y} \sum_{i=1}^{N_1} r_i^2 \frac{dI_{\text{cable}}}{dt} \\ &\approx 0.0059 \cos(2\pi f_p t) \text{V} \end{aligned} \tag{21}$$

where f_{p} is the power frequency. It can be seen that $U_{\text{cable2coil}}$ generated by the PFMF is very small, so the normal working state of the domino-coils WPT system is basically free from the interference of the power line.

At last, upon comparing the efficiency improvement researches of domino-coils WPT systems outlined in Table IV, it is evident that the maximum coupling coefficient and quality factor of single-layer domino-coils presented in this study surpass those of previous investigations. Additionally, a coefficient termed volume divided by distance (VDD), defined as the total

TABLE IV
COMPARISON WITH EXISTING RESEARCH

Ref	Coil Size	Distance	Winding Type	Coil number	VDD	Maximum coupling coefficient K	Quality factor Q	Maximum PTE	Power
[21]	Φ200 mm×1.6 mm	110 cm	Two-layer PCB winding	13	5.94	-	64	11%	6 W
[22]	Φ198 mm×1.5 mm	114 cm	Two-layer PCB winding	13	5.26	0.14	132	46%	20 W
[23]	Φ198 mm×1.6 mm	38 cm	Single-layer and double-layer PCB winding	5	6.61	0.126	144	55.2%	16.3 W
[20]	Φ250 mm×180 mm	250 cm	Double-layer CSC with ferrite	5	176.63	0.019	607	66.7%	8.89 W
[1]	Φ176 mm×3.4 mm	110 cm	Two-layer planar winding with Litz wire	12	9.02	-	300	60%	25 W
[13]	Φ200 mm×14 mm	70 cm	Three-layer planar winding with Litz wire	8	50.24	0.144	350	70%	25 W
[27]	Φ 200 mm×4 mm	40 cm	Two-layer planar winding with Litz wire	5	15.7	0.129	108	87.5%	20 W
[28]	Φ170 mm	150 cm	Planar winding with Litz wire	10	-	0.036	617	42%	1.34 W
[29]	Φ200 mm×6 mm	25 cm	Three-layer planar winding with Litz wire	6	45.22	0.31	302	84.2%	25 W
[31]	320 mm×320 mm×1.4 mm	50 cm	One-layer square winding with Litz wire	3	27.02	0.115	434	81.95%	37.86 W
This work	Φ200 mm×2 mm	50 cm	One-layer planar winding with Litz wire	7	8.79	0.154	Average:566 Maximum:759	85.94%	12.23 W

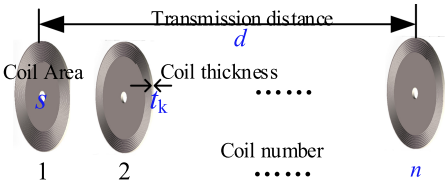

Fig. 19. VDD coefficient definition.

coil volume divided by the transmission distance, provides insight into the spatial relationship between the domino-coils and the transmission distance. The diagram of the VDD coefficient definition is shown in Fig. 19.

Equation (22) gives the calculation of VDD coefficient

$$\mathrm{VDD} = \mathrm{CoilVolume}/\mathrm{Distance} = st_{\mathrm{k}}n/d \tag{22}$$

where s represents the area of the coil plane, t_{k} represents the coil thickness, and d is the transmission distance.

A smaller VDD signifies less spatial occupation within the insulator, which is more conducive to meeting the miniaturization requirements of the domino-coils. The VDD of single-layer domino-coils in this article is 8.79, generally lower than that of multilayer planar Litz winding. Furthermore, it exhibits a higher PTE of 85.94% at an output power of 12.23 W.

V. CONCLUSION

This article investigates the optimal configuration of single-layer domino-coils with uniform spacing for online monitoring equipment. An optimal efficiency condition for arbitrary number of domino-coils is proposed using the T equivalent circuit and its gyrator characteristics, namely the current ratio of nonadjacent coils equaling the mutual inductance ratio of adjacent coils. Single-layer domino-coils with uniform spacing is further optimized by independently adjusting the parameters of each coil based on the proposed optimal efficiency condition. Experimental verification are provided to demonstrate the efficiency improvement, and a dc output of 12.23 W with an efficiency of 85.94% is achieved at a distance of 50 cm. This work not only promotes the coupling coefficient and quality factor of domino-coils, but also minimizes the total space occupied by the domino-coils.

By mathematical analysis and experimental verification on single-layer domino-coils, the crucial coupling relation determinant that are S_3 and S_4 in a seven domino-coils WPT system, and the errors between current ratio and mutual inductance ratio involving S_3 and S_4 should be as small as possible to ensure the high-efficiency power transmission. Although other coupling relations such as S_1, S_5, and S_2 are proved with low sensitivity to system transmission efficiency, research on ways is needed to inhibit or eliminate the cross-coupling among them to further improve the output performance of domino-coils WPT system.

REFERENCES

[1] C. Cai et al., "Resonant wireless charging system design for 110-kV high-voltage transmission line monitoring equipment," *IEEE Trans. Ind. Electron.*, vol. 66, no. 5, pp. 4118–4129, May 2019.
[2] L. Du, C. S. Wang, X. Z. Li, L. J. Yang, Y. Mi, and C. X. Sun, "A novel power supply of online monitoring systems for power transmission lines," *IEEE Trans. Ind. Electron.*, vol. 57, no. 8, pp. 2889–2895, Aug. 2010.
[3] P. Li, Y. M. Wen, Z. Q. Zhang, and S. Q. Pan, "A high-efficiency management circuit using multiwinding upconversion current transformer for power-line energy harvesting," *IEEE Trans. Ind. Electron.*, vol. 62, no. 10, pp. 6327–6335, Oct. 2015.
[4] W. Wang, X. L. Huang, L. L. Tan, J. F. Zhao, and C. X. Yan, "Hybrid wireless charging system for monitoring overhead 110 kV high-voltage power line equipment based on magneto-electric conversion," *IET Gener. Transmiss. Distrib.*, vol. 10, no. 5, pp. 1199–1208, Apr. 2016.
[5] C. Zhang, N. Tang, W. X. Zhong, C. K. Lee, and R. S. Y. Hui, "A new energy harvesting and wireless power transfer system for smart grid," in *Proc. IEEE 7th Int. Symp. Power Electron. Distrib. Gener. Syst.*, Jun. 2016, pp. 1–5.
[6] Z. Liu, Y. Li, N. Duan, and Z. He, "An energy management method for magnetic field energy harvesters under wide-range current in railway electrification systems," *IEEE Trans. Ind. Electron.*, vol. 71, no. 5, pp. 5360–5369, May 2024.
[7] C. Zhang, D. Lin, N. Tang, and S. Y. R. Hui, "A novel electric insulation string structure with high-voltage insulation and wireless power transfer capabilities," *IEEE Trans. Power Electron.*, vol. 33, no. 1, pp. 87–96, Jan. 2018.
[8] W. Zhong, C. K. Lee, and S. Y. R. Hui, "General analysis on the use of Tesla's resonators in domino forms for wireless power transfer," *IEEE Trans. Ind. Electron.*, vol. 60, no. 1, pp. 261–270, Jan. 2013.
[9] D. Ahn and S. Hong, "A study on magnetic field repeater in wireless power transfer," *IEEE Trans. Ind. Electron.*, vol. 60, no. 1, pp. 360–371, Jan. 2013.
[10] D. H. Tran, V. B. Vu, and W. Choi, "Design of a high-efficiency wireless power transfer system with intermediate coils for the on-board chargers of electric vehicles," *IEEE Trans. Power Electron.*, vol. 33, no. 1, pp. 175–187, Jan. 2018.
[11] Z. Zhang, H. Pang, A. Georgiadis, and C. Cecati, "Wireless power transfer—An overview," *IEEE Trans. Ind. Electron.*, vol. 66, no. 2, pp. 1044–1058, Feb. 2019.
[12] Q. Deng et al., "Frequency-dependent resistance of litz-wire square solenoid coils and quality factor optimization for wireless power transfer," *IEEE Trans. Ind. Electron.*, vol. 63, no. 5, pp. 2825–2837, May

[13] Z. Dong, S. Liu, X. Li, Z. Xu, and L. Yang, "A novel long-distance wireless power transfer system with constant current output based on domino-resonator," *IEEE J. Emerg. Sel. Topics Power Electron.*, vol. 9, no. 2, pp. 2343–2355, Apr. 2021.
[14] L. Zhou, R. Mai, S. Liu, J. Yu, Y. Li, and L. Fu, "Minimizing input current of the rectifier of LCC–LCC compensated IPT systems by switch-controlled capacitor for improving efficiency," *IEEE Trans. Ind. Appl.*, vol. 58, no. 1, pp. 1010–1021, Jan./Feb. 2022.
[15] Y. Guo and Y. Zhang, "Secondary side voltage and current estimation of wireless power transfer systems," *IEEE Trans. Ind. Appl.*, vol. 58, no. 1, pp. 1222–1230, Jan./Feb. 2022.
[16] C. Cai, J. Wang, M. Saeedifard, P. Zhang, R. Chen, and J. Zhang, "Gyrator-gain variable WPT topology for MC-unconstrained CC output customization using simplified capacitance tuning," *IEEE Trans. Ind. Electron.*, vol. 71, no. 4, pp. 3594–3605, Apr. 2024.
[17] Y. H. Sohn, B. H. Choi, G.-H. Cho, and C. T. Rim, "Gyrator-based analysis of resonant circuits in inductive power transfer systems," *IEEE Trans. Power Electron.*, vol. 31, no. 10, pp. 6824–6843, Oct. 2016.
[18] F. Lu et al., "A high-efficiency and long-distance power-relay system with equal power distribution," *IEEE J. Emerg. Sel. Topics Power Electron.*, vol. 8, no. 2, pp. 1419–1427, Jun. 2020.
[19] P. Gu et al., "A three-stage-five-coil IPT system based on cylindrical solenoid coupler applied to State detection equipment of HV device," *IEEE Trans. Power Electron.*, vol. 37, no. 2, pp. 2382–2393, Feb. 2022.
[20] P. Gu et al., "A 2.5m long-range IPT system based on Domino cylindrical solenoid coupler compensated respectively in layers," *IEEE Trans. Ind. Electron.*, vol. 70, no. 2, pp. 1409–1420, Feb. 2023.
[21] J. Qu, L. He, N. Tang, and C.-K. Lee, "Wireless power transfer using Domino-resonator for 110-kV power grid online monitoring equipment," *IEEE Trans. Power Electron.*, vol. 35, no. 11, pp. 11380–11390, Nov. 2020.
[22] Y. Fang, J. Qu, B. M. H. Pong, C. K. Lee, and R. S. Y. Hui, "Quasi-static modeling and optimization of two-layer PCB resonators in wireless power transfer systems for 110-kV power grid online monitoring equipment," *IEEE Trans. Ind. Electron.*, vol. 69, no. 2, pp. 1400–1410, Feb. 2022.
[23] J. Zhou, Z. Li, C.-K. Lee, K. W. Chan, and S. Y. R. Hui, "A weather-independent and renewable power supply with wireless power transfer feature for powering online monitoring systems in smart grid," *IEEE Trans. Ind. Electron.*, vol. 70, no. 6, pp. 6414–6424, Jun. 2023.
[24] K. Lee and S. H. Chae, "Power transfer efficiency analysis of intermediate-resonator for wireless power transfer," *IEEE Trans. Power Electron.*, vol. 33, no. 3, pp. 2484–2493, Mar. 2018.
[25] C. K. Lee, W. X. Zhong, and S. Y. R. Hui, "Effects of magnetic coupling of nonadjacent resonators on wireless power domino-resonator systems," *IEEE Trans. Power Electron.*, vol. 27, no. 4, pp. 1905–1916, Apr. 2012.
[26] Y. Liu, J. Chen, Y. Li, and Z. He, "A new modeling method for multiple-relay wireless power transfer system considering cross-coupling," *IEEE Trans. Ind. Electron.*, vol. 71, no. 2, pp. 1456–1467, Feb. 2024.
[27] Y. Liu, Y. Li, X. Zhang, and Z. He, "Load-independent voltage-gain design method for domino-resonator wireless power transfer systems," *IEEE Trans. Power Electron.*, vol. 39, no. 2, pp. 1997–2003, Feb. 2024.
[28] Y. Guan, Y. Xiao, Y. Cui, and D. Xu, "Analysis and optimal design of Mid-range WPT system based on multiple repeaters," *IEEE Trans. Ind. Appl.*, vol. 58, no. 1, pp. 1092–1100, Jan./Feb. 2022.
[29] X. Hou, H. Hu, Y. Su, Z. Liu, Z. Deng, and R. Deng, "A multirelay wireless power transfer system with double-sided LCC compensation network for online monitoring equipment," *IEEE J. Emerg. Sel. Topics Power Electron.*, vol. 11, no. 1, pp. 1262–1271, Feb. 2023.
[30] R. P. Wojda and M. K. Kazimierczuk, "Winding resistance and power loss of inductors with litz and solid-round wires," *IEEE Trans. Ind. Appl.*, vol. 54, no. 4, pp. 3548–3557, Jul./Aug. 2018.
[31] X. Shu, B. Zhang, Z. Wei, C. Rong, and S. Sun, "Extended-distance wireless power transfer system with constant output power and transfer efficiency based on parity-time-symmetric principle," *IEEE Trans. Power Electron.*, vol. 36, no. 8, pp. 8861–8871, Aug. 2021.

Yanling Li (Member, IEEE) received the B.Sc. and Ph.D. degrees in control theory and control engineering from Chongqing University, Chongqing, China, 2008 and 2012, respectively.

She is currently an Associate Professor with the School of Electrical Engineering, Southwest Jiaotong University, Chengdu, China. She is a Guest Editor of Electronics for a special issue "Wireless Power Transfer and Its Applications". Her research interests include wireless power transfer and its applications, power electronic system modeling and control.

Li Gui received the B.Sc. degree in electrical engineering and automation from Northeast Petroleum University, Heilongjiang, China, 2021. She is currently working toward the M.Sc. degree in electrical engineering with Southwest Jiaotong University, Chengdu, China.

Her main research interest includes wireless power transfer and its applications.

Yongkang Jiang received the B.Sc. degree in ship electronic and electrical engineering from Shanghai Maritime University, Shanghai, China, 2022. He is currently working toward the M.Sc. degree in electrical engineering with Southwest Jiaotong University, Chengdu, China.

His main research interest includes wireless power transfer technology.

Rui Jing received the B.Sc. degree in electrical engineering and automation in 2021 from Southwest Jiaotong University, Chengdu, China, where he is currently working toward the M.Sc. degree in electrical engineering.

His main research interest includes wireless power transfer technology.

Yong Li (Senior Member, IEEE) received the B.Sc. and Ph.D. degrees in electrical engineering from the School of Electrical Engineering, Southwest Jiaotong University, Chengdu, China, in 2013 and 2017, respectively.

From 2017 to 2018, he was a Research Associate with the Department of Electrical Engineering, The Hong Kong Polytechnic University, where he was a Postdoctoral Fellow. He is currently an Associate Professor with Southwest Jiaotong University, Chengdu, China. He is a Guest Editor of Electronics for a special issue "Wireless Power Transfer and Its Applications". His main research interests include wireless power transfer and energy harvesting.

Zhengyou He (Senior Member, IEEE) received the B.Sc. and M.Sc. degrees in computational mechanics from Chongqing University, Chongqing, China, in 1992 and 1995, respectively, and the Ph.D. degree in power system and automation from the School of Electrical Engineering, Southwest Jiaotong University, Chengdu, China, in 2001.

He is currently a Professor with the School of Electrical Engineering, Southwest Jiaotong University. His research interests include signal process and information theory applied to electrical power system, and application of wavelet transforms in power systems.